

Nonmonotonic anomalous Hall effect and anisotropic magnetoresistance in $SrRuO_3/PbZr_{0.52}Ti_{0.48}O_3$ heterostructures

Zhen-Li Wang(王振礼), Chao-Yang Kang(康朝阳), Cai-Hong Jia(贾彩虹), Hai-Zhong Guo(郭海中), and Wei-Feng Zhang(张伟风)

Citation: Chin. Phys. B, 2023, 32 (**10**): 107303. DOI: 10.1088/1674-1056/accd58

Journal homepage: http://cpb.iphy.ac.cn; http://iopscience.iop.org/cpb

What follows is a list of articles you may be interested in

Moiré Dirac fermions in transition metal dichalcogenides heterobilayers

Chenglong Che(车成龙), Yawei Lv(吕亚威), and Qingjun Tong(童庆军)
Chin. Phys. B, 2023, 32 (**10**): 107307. DOI: 10.1088/1674-1056/aceee5

Resistive switching properties of SnO_2 nanowires fabricated by chemical vapor deposition

Ya-Qi Chen(陈亚琦), Zheng-Hua Tang(唐政华), Chun-Zhi Jiang(蒋纯志), and De-Gao Xu(徐德高)
Chin. Phys. B, 2023, 32 (**9**): 097302. DOI: 10.1088/1674-1056/acc3fd

Nonlinear current response and electric quantum oscillations in the Dirac semimetal Cd_3As_2

Hao-Nan Cui(崔浩楠), Ze-Nan Wu(吴泽南), Jian-Kun Wang(王建坤), Guang-Yu Zhu(祝光宇), Jia-Jie Yang(杨佳洁), Wen-Zhuang Zheng(郑文壮), Zhi-Min Liao(廖志敏), Shuo Wang(王硕), Ben-Chuan Lin(林本川), and Dapeng Yu(俞大鹏)
Chin. Phys. B, 2023, 32 (**8**): 087306. DOI: 10.1088/1674-1056/acd9c5

On the Onsager-Casimir reciprocal relations in a tilted Weyl semimetal

Bingyan Jiang(江丙炎), Jiaji Zhao(赵嘉佶), Lujunyu Wang(王陆君瑜), Ran Bi(毕然), Juewen Fan(范珏雯), Zhilin Li(李治林), and Xiaosong Wu(吴孝松)
Chin. Phys. B, 2022, 31 (**9**): 097306. DOI: 10.1088/1674-1056/ac754a

Topological transport in Dirac electronic systems: A concise review

Hua-Ding Song(宋化鼎), Dian Sheng(盛典), An-Qi Wang(王安琦), Jin-Guang Li(李金光), Da-Peng Yu(俞大鹏), Zhi-Min Liao(廖志敏)
Chin. Phys. B, 2017, 26 (**3**): 037301. DOI: 10.1088/1674-1056/26/3/037301

Nonmonotonic anomalous Hall effect and anisotropic magnetoresistance in $SrRuO_3/PbZr_{0.52}Ti_{0.48}O_3$ heterostructures

Zhen-Li Wang(王振礼)[1], Chao-Yang Kang(康朝阳)[1], Cai-Hong Jia(贾彩虹)[1], Hai-Zhong Guo(郭海中)[2,†], and Wei-Feng Zhang(张伟风)[1,‡]

[1] *Center for Topological Functional Materials, Henan University, Kaifeng* 475004, *China*
[2] *Key Laboratory of Material Physics (Ministry of Education), School of Physics and Microelectronics, Zhengzhou University, Zhengzhou* 450052, *China*

(Received 20 February 2023; revised manuscript received 4 April 2023; accepted manuscript online 17 April 2023)

We fabricate $SrRuO_3/PbZr_{0.52}Ti_{0.48}O_3$ heterostructures each with an in-plane tensile-strained $SrRuO_3$ layer and investigate the effect of an applied electric field on anomalous Hall effect. The four-fold symmetry of anisotropic magnetoresistance and the nonmonotonic variation of anomalous Hall resistivity are observed. By applying positive electric field or negative electric field, the intersecting hump-like feature is suppressed or enhanced, respectively. The sign and magnitude of the anomalous Hall conductivity can be effectively controlled with an electric field under a high magnetic field. The electric-field-modulated anomalous Hall effect is associated with the magnetization rotation in $SrRuO_3$. The experimental results are helpful in modulating the magnetization rotation in spintronic devices based on $SrRuO_3$ heterostructures.

Keywords: Berry curvature, electric field, anomalous Hall effect, anisotropic magnetoresistance, magnetization rotation

PACS: 73.43.–f, 73.43.Qt, 75.60.Jk **DOI:** 10.1088/1674-1056/accd58

1. Introduction

Berry curvature in the conduction band of materials is an important physical concept in modern condensed matter physics, which is closely related to many novel physical properties of ferromagnetic materials.[1–4] When studying the Hall effect, the Berry curvature for magnetic material can be considered as a magnetic field in momentum space, leading to many interesting magnetotransport phenomena.[5–7] For example, it is well known that for the anomalous Hall effect (AHE) and the topological Hall effect (THE) in ferromagnet,[2,8–10] the anomalous Hall conductivity ($\sigma_{xy}^{\mathrm{AHE}}$) is directly proportional to the Berry curvature integral of all occupied electron bands in Brillouin zone.[11] The amplitude and sign of $\sigma_{xy}^{\mathrm{AHE}}$ are especially sensitive to the electronic band structure, particularly in a ferromagnetic material with significant spin-orbit coupling.[12,13] In transition metal oxides, the coupling effects between lattice, charge, orbit, and spin degree of freedom greatly affect electronic structures, thus affecting the physical properties of materials.[14–16] Therefore, the strain and electric field can be considered as an effective method to modulate the Berry curvature and AHE.

Perovskite oxides have been widely studied because of their intriguing and rich physical properties, such as superconductivity, magnetism, ferroelectricity, Berry curvature, and so on.[17–20] $SrRuO_3$ (SRO) is the only 4d transition metal oxide with ferromagnetism and metallicity among the many perovskite-structured oxides known to date. In SRO, the THE induced by skyrmions and the AHE related to Berry curvature have been reported.[19,21–26] Ren *et al.* observed nonmonotonic behavior formed by the superposition of positive and negative polarity AHE signals in $BiFeO_3/SrRuO_3$ heterostructures.[27] Mizuno *et al.* reported the realization of gating-induced changes in Berry curvature integral over the filled electronic states in $BaTiO_3/SrRuO_3$ heterostructures.[28] Recently, Tian *et al.* demonstrated that the change of Berry curvature is closely related to the magnitude of the in-plane tensile strain or compressive strain of the SRO film.[29] In SRO films or related heterostructures, non-monotonic AHE behavior, which is directly related to the evolution of spin-rotating Berry curvature, has been observed only in SRO films grown on $DyScO_3$ substrates so far. The magnetization also changes with the external magnetic field. If the simultaneous modulation can be realized by strain and gating, it is not only helpful in building novel low-power spintronic devices but also an effective research strategy to achieve the modulation of Berry curvature and to explore the physical phenomena related to the magnetization rotation. Therefore, it is more than essential to further investigate the effects of epitaxial strain and electric field associated with ferroelectric $Pb(Zr,Ti)O_3$ on nonmonotonic AHE and magnetization rotation in SRO films.

[†]Corresponding author. E-mail: hguo@zzu.edu.cn
[‡]Corresponding author. E-mail: wfzhang@henu.edu.cn

© 2023 Chinese Physical Society and IOP Publishing Ltd

In the present study, we observed the strain-induced nonmonotonic anomalous Hall effect and the four-fold symmetry anisotropic magnetoresistance simultaneously in $SrRuO_3/PbZr_{0.52}Ti_{0.48}O_3/La_{0.7}Sr_{0.3}MnO_3$ heterostructures. We further revealed that the electric field can modulate the Berry curvature by inducing the rotation of the magnetization. Both the magnitude and sign of the anomalous Hall resistivity (ρ_{xy}^{AHE}) can be effectively modulated by an electric field, which arises from the electric field-induced magnetization rotation in SRO, which further induces Berry curvature evolution. This work suggests that the strain and electric field manipulation of ρ_{xy}^{AHE} can be an effective pathway to explore the relationship between Berry curvature and magnetization rotation in SRO heterostructures.

2. Methods

The SRO, $PbZr_{0.52}Ti_{0.48}O_3$ (PZT), and $La_{0.7}Sr_{0.3}MnO_3$ (LSMO) films were deposited by the pulsed laser deposition (PLD, Adnano-Tek). The $SrTiO_3$ (STO) substrate was pretreated according to the procedure described in our previous work[30] to obtain TiO_2-terminated surfaces. The SRO ($\sim$ 20 nm), PZT ($\sim$ 90 nm), and LSMO ($\sim$ 10 nm) films were grown at 650 °C under an oxygen partial pressure of 10 Pa (the laser wavelength of 248 nm, the pulse repetition rate of 2 Hz, and the laser energy density of 1.8 J/cm^2). Figure 1(a) shows the schematic diagram of the SRO/PZT/LSMO heterostructure grown on a TiO_2-terminated $SrTiO_3$ (001) substrate. X-ray diffraction (XRD, Bruker D8 advance) with Cu $K\alpha$ radiation was performed to determine the crystalline state of film. Surface morphology and ferroelectric property were investigated by a scanning probe microscope (SPM, Asylum Research 3D Infinity) with a conductive tip. The Hall effect and magnetoresistance were measured in a physical property measurement system (PPMS-9) with a rotator module. To obtain the angular dependence of the resistivity, the sample orientation was varied with magnetic field under a certain temperature and magnetic field.

3. Results and discussion

Figure 1(b) shows the XRD θ–2θ scanning pattern of the SRO/PZT/LSMO heterostructure, where the (00l) diffraction peaks from the PZT film and the STO substrate are clearly observed. The diffraction peaks of SRO and LSMO films can be clearly seen in the enlarged region between the angles 42° and 49° in the inset of Fig. 1(b). According to the Bragg diffraction equation, the lattice constant of the c axis of the SRO film can be calculated to be about 3.924 Å. Since the lattice constant of the bulk SRO is 3.930 Å, the out-of-plane compressive strain in the SRO film of -0.15% is obtained. Furthermore, the in-plane tensile strain of 0.16% is achieved from the Poisson ratio of 0.32.[31] As shown by the atomic force microscope measurement shown in Fig. 1(c), the surface of SRO/PZT/LSMO is quite flat, with a roughness of about 0.4 nm, implying that a high-quality SRO/PZT/LSMO heterostructure is obtained.

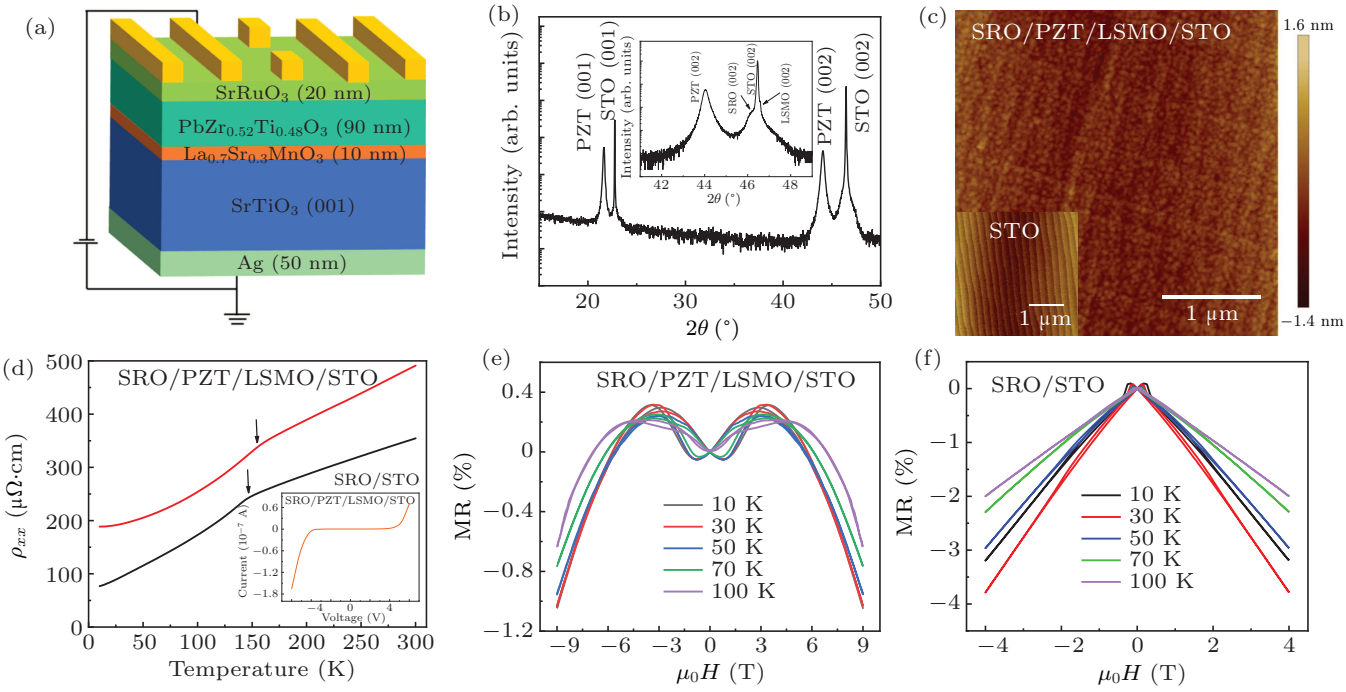


Fig. 1. (a) The schematic diagram, (b) the XRD pattern, (c) the AFM height topographic images of the SRO/PZT/LSMO heterostructure (image size: 3 μm×3 μm), (d) the temperature-dependent longitudinal resistivity (ρ_{xx}–T) and I–V curves of the SRO/PZT/LSMO heterostructure, (e) the magnetic field-dependent MR of SRO/PZT/LSMO heterostructure at different temperatures, and (f) the magnetic field-dependent MR of the SRO film at different temperatures.

As shown in Fig. 1(a), the LSMO conductive layer is completely covered by the ferroelectric insulating layer PZT. Moreover, the insulating behavior is demonstrated in the SRO/PZT/LSMO heterostructure in the inset of Fig. 1(c). Therefore, we can rule out the influence of the LSMO layer on the SRO/PZT/LSMO heterostructure in the transport measurement. Figure 1(d) shows the temperature dependence of the longitudinal resistivity of the SRO/STO sample and the SRO/PZT/LSMO/STO sample. A clear kink at 148 K can be observed for SRO/STO, which is consistent with the previously reported result in SRO film.[16,32,33] For SRO/PZT/LSMO/STO, a weak kink at 157 K is observed. The kink corresponds to the Curie temperature (T_C), at which the phase transition from the paramagnetic to the ferromagnetic state occurs. The T_C value of the in-plane tensile-strained SRO film is higher than that of the in-plane compressive-strained SRO film on the STO substrate, which is consistent with previous result about the enhancement of T_C by tensile strain.[34] Figure 1(e) shows the magnetic-field dependence of magnetoresistance (MR) [MR $= (R_H - R)/R$)], which is measured at temperatures ranging from 10 K to 100 K. For the SRO/PZT/LSMO heterostructure, the out-of-plane MR exhibits a nonmonotonic variation, with positive MR observed in the low magnetic field region. This result is in agreement with the previous result of SRO film with in-plane tensile strain.[14,19] As shown in Fig. 1(f), for the SRO film grown on STO substrates under compressive strain, we can observe standard negative MR with butterfly-shaped hysteresis. These clearly indicate that there are two competing MR mechanisms in the SRO/PZT/LSMO heterostructure at different temperatures. The positive MR effect in low magnetic field and the negative MR effect in high magnetic field cause magnetic easy axis to deviate from out-of-plane with the increase of magnetic field. This point will be further clarified by the anisotropic magnetoresistance (AMR) measurements.

The schematic diagram for the AMR measurement is shown in Fig. 2(a). To demonstrate that the magnetic easy axis of the SRO/PZT/LSMO heterostructure lies in the plane, we perform θ-dependent AMR measurements. The angle θ is defined as the angle between the magnetic field and the film's normal direction in the (010) plane, and $\theta = 0^\circ$ defined as the external magnetic field H perpendicular to the film surface. The reversal of magnetization leads to peaks in ρ_{xx} around the easy axis when the angle between the easy axis and the field exceeds 90°.[29,35,36] The AMR of the SRO/PZT/LSMO heterostructure shows hysteretic peaks near $\theta = 180^\circ$ [see Fig. 2(b)], indicating that the magnetic easy axis is close to the in-plane direction, which accords with an in-plane tensile strain derived from the XRD measurement. On the contrary, the AMR of the SRO film shows two hysteresis peaks near $\theta = 90^\circ$ and 270°, respectively [see Fig. 2(c)], implying that the magnetic easy axis is close to the out-of-plane direction, which is consistent with the previous result.[35] Then, we perform φ-dependent AMR measurements. The angle φ is defined as the angle between the magnetic field and the film's normal direction in the (100) plane, and $\varphi = 0^\circ$ is defined as the external magnetic field H perpendicular to the film surface. Figures 2(d)–2(f) show the angle (φ)-dependent AMR of the SRO/PZT/LSMO heterostructure at 40 K under the magnetic fields of 1 T, 4 T, and 8 T, respectively. Under a low magnetic field of 1 T, the AMR curve shows a two-fold symmetry, and it presents a four-fold symmetry feature under a high magnetic field of 4 T. The four-fold symmetry feature of the AMR curve is more pronounced at higher magnetic fields. The AMR curve can be well fitted by the following equation:

$$\begin{aligned} \mathrm{AMR} &= \frac{R(\varphi) - R(0)}{R(0)} \times 100\,\% \\ &= C_0 + C_{2\varphi}\cos(2\varphi + \varphi_1) + C_{4\varphi}\cos(4\varphi + \varphi_2), \quad (1) \end{aligned}$$

where $C_{2\varphi}$ and $C_{4\varphi}$ represent the amplitude of two-fold and four-fold symmetric AMR, respectively, C_0, φ_1, and φ_2 are the coefficients.[36–39] It turns out that the above AMR curves can be fitted very well by Eq. (1). According to the spin dependent scattering theory,[40,41] the resistivity of a magnetic system is closely related to the alignments of spin moments and the free energy as well. The free energy of a system includes magnetocrystalline anisotropy energy (E_K), Zeeman energy (E_H), and exchange energy (E_{ex}), i.e., $E = E_K + E_H + E_{ex}$.[42] For a fully magnetized ferromagnetic system, the magnetic moments point to the same direction at the same time, and the exchange energy is negligible. The magnetocrystalline anisotropy energy varies along crystal axis direction in high magnetic field. The easy axis has the lowest magnetocrystalline anisotropy energy, while the hard axis has the highest one. The Zeeman energy in ferromagnetic system is related to the applied magnetic field. When the magnetic moment points to the same direction as the external field direction, the Zeeman energy reaches its lowest value. Therefore, for the SRO/PZT/LSMO heterostructure, the main attribution to AMR is E_K and E_H. We speculate that the four-fold symmetric behavior in the AMR curve results from the rotation of the magnetization due to the competition between the magnetocrystalline anisotropy energy and the Zeeman energy.[39] The two-fold symmetric AMR is mainly attributed to the uniaxial anisotropy with the easy axis lying in the plane. With the increase of the magnetic field, SRO forms a spin canting state and the magnetization tends to align along the external field magnetic direction, albeit with some deviation.[43] When the magnetic field is perpendicular to the heterostructure plane, the equivalent spin-canting state will appear both at the angle above or below 90°, which means that the two AMR peaks will be revealed in the vicinity of 90° and a minimum AMR

will be at 90°. When the angle (φ) is rotated to 90°, the magnetic field is parallel to the SRO/PZT/LSMO heterostructure plane. The spins tend to be arranged regularly in the plane, so the AMR is in a low state. Thus, a clear four-fold dominant symmetric AMR is observed under a high magnetic field of 8 T at the low temperature of 40 K.

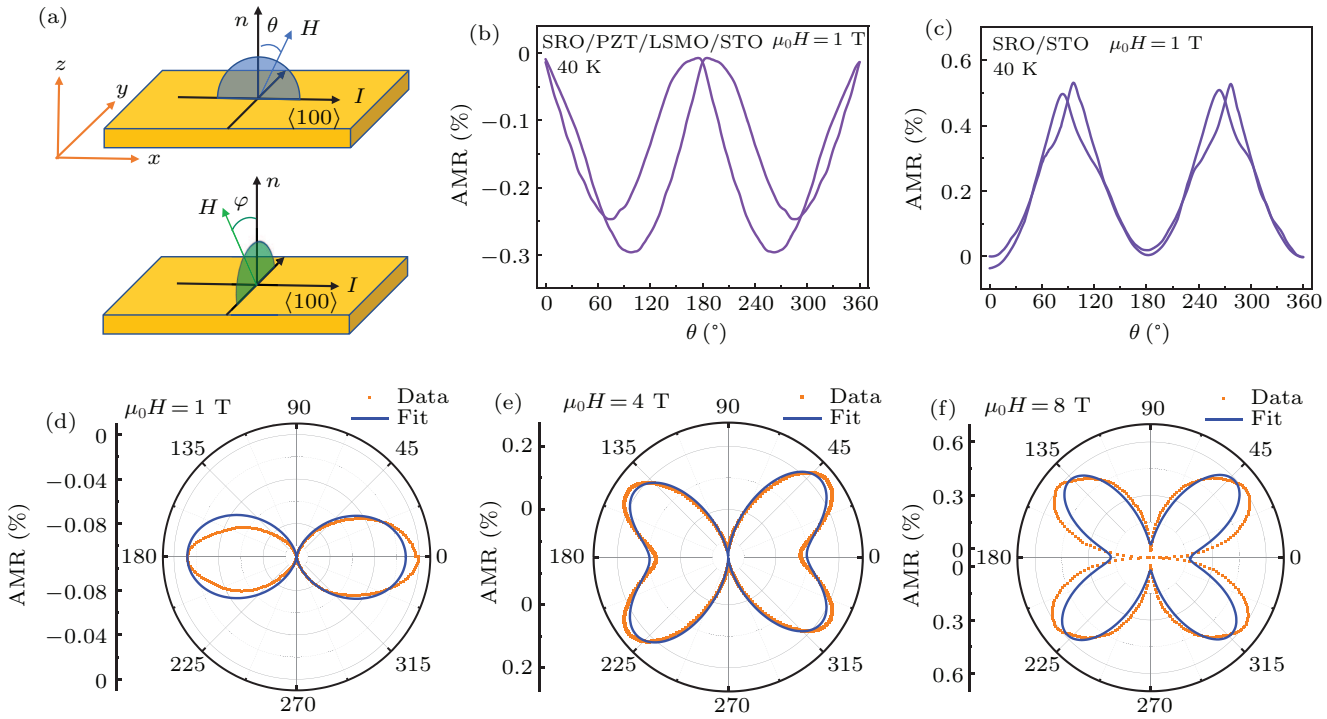


Fig. 2. (a) Schematic diagram of out-of-plane anisotropic magnetoresistance measurement. Angular θ-dependent AMR for (b) SRO/PZT/LSMO heterostructures and (c) SRO films measured at 40 K with $\mu_0 H = 1$ T, with angular φ-dependent AMR of SRO/PZT/LSMO heterostructures measured at (d) 1 T, (e) 4 T, and (f) 8 T at 40 K, and blue solid lines representing fitting results.

In general, the Hall resistivity can be decomposed into $\rho_{xy} = \rho_{\mathrm{OHE}} + \rho_{\mathrm{AHE}}$, where ρ_{OHE} and ρ_{AHE} denote the ordinary and anomalous Hall resistivity, respectively.[11,31,44] In a ferromagnet, the ordinary Hall resistivity is proportional to the out-of-plane applied magnetic field (H_z), i.e. $\rho_{\mathrm{OHE}} = R_0 H_z$, which is caused by the classical Lorentz force; the anomalous Hall resistivity is proportional to the out-of-plane component of magnetization (M_z), i.e. $\rho_{\mathrm{AHE}} = R_{\mathrm{S}} M_z$.[21,45] For SRO, it is generally believed that AHE is caused by an intrinsic mechanism. Under the action of spin–orbit coupling, the carriers in the occupied state of the SRO band will have an additional abnormal velocity in an external electric field. When the spin-up and spin-down electron occupancy numbers are unequal, a net lateral current is generated in the SRO.[46] The R_{S} is proportional to the longitudinal resistivity ρ_{xx}^2. Both the sign and magnitude of ρ_{AHE} are related to the magnetization M. The sign and magnitude of the magnetization M vary with the external magnetic field. The temperature-dependent AHE of SRO/PZT/LSMO heterostructures and SRO film are shown in Fig. 4, in which the contribution of the ordinary Hall effect to the total Hall resistivity is removed by linear fitting ρ_{xy} in the higher magnetic-field region. In Fig. 4(a), the SRO/PZT/LSMO heterostructure exhibits a strong temperature-dependent behavior with the following two characteristics. (i) The intersecting hump-like features (located in the intermediate magnetic field region from 3 T to 6 T or −3 T to −6 T) can be clearly seen, where the size of the features becomes weaker with temperature increasing until it disappears completely. (ii) The ρ_{xy}^{AHE} nonmonotonically changes with magnetic field, and the sign is reversed from positive to negative with temperature increasing at a high magnetic field of −9 T. These two characteristics indicate that the PZT can significantly modulate the AHE of SRO film. Figure 3(b) shows the magnetic-field dependence of ρ_{xy}^{AHE} in the SRO film in the range of 10 K to 100 K. In contrast, the sign of ρ_{xy}^{AHE} under the saturated magnetic field is not reversed with temperature increasing. To gain an insight into the nonmonotonic behavior with the magnetic field and the intersecting hump-like features of the ρ_{xy}^{AHE} in the SRO/PZT/LSMO heterostructure, we conduct an in-depth analysis of the ρ_{xy}^{AHE} curve at 40 K. In Fig. 3(c), the ρ_{xy}^{AHE} increases with the sign reversal from negative to positive with magnetic field decreasing from −9 T to 0 T; as the magnetic field increases from 0 T to 9 T, the ρ_{xy}^{AHE} rises to a maximum value at ∼ 0.55 T, and then begins to decrease with the sign reversing from back to negative sign and reaches a minimum value at ∼ 2.7 T, and after that it increases with the sign reversing to positive at a high magnetic field of ∼ 6 T. A similar but opposite change behavior can be observed as the magnetic field varies from 9 T to

−9 T in Fig. 3(c). The rotation of the magnetic moment in real space of an in-plane tensile-strain can result in a nonmonotonic change of anomalous Hall resistivity with the sweeping of magnetic field.[29] Zeeman energy tends to make the magnetic moment lie in the same direction as the external magnetic field. In other words, as the external magnetic field increases, the magnetization M gradually rotates from in-plane to out-of-plane direction. Therefore, the ρ_{xy}^{AHE} of the SRO/PZT/LSMO heterostructure also exhibits a non-monotonic variation with the external magnetic field. In Fig. 3(d), the ρ_{xy}^{AHE} curve exhibits a typical square-shaped hysteresis. Via a ferroelectric PZT buffer layer, therefore, the AHE can be effectively modulated, and a nonmonotonic change of the ρ_{xy}^{AHE} can occur in the SRO film.

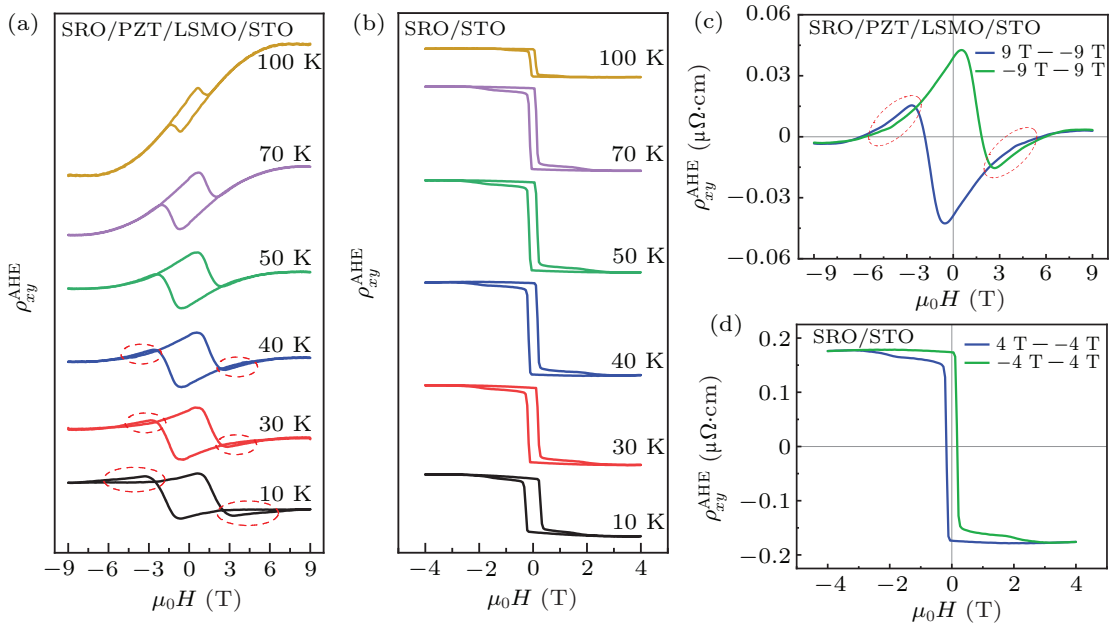


Fig. 3. Magnetic field-dependent transverse Hall resistivity curves (ρ_{xy}^{AHE}–$\mu_0 H$) of (a) SRO/PZT/LSMO heterostructures, (b) SRO films measured from 10 K to 100 K, with ordinary Hall term ($R_0 H$) s subtracted by linear fitting at a higher magnetic field, and an offset applied for each ρ_{xy}^{AHE}–$\mu_0 H$ curve for clarity, (c) ρ_{xy}^{AHE}–$\mu_0 H$ curves for SRO/PZT/LSMO heterostructures at 40 K, and (d) ρ_{xy}^{AHE}–$\mu_0 H$ curves for SRO films at 40 K.

We further investigate the effect of the polarization electric field on the ρ_{xy}^{AHE} in SRO/PZT/LSMO heterostructure. We choose the Ag electrode on the back of the STO as a bottom electrode and the SRO as a top electrode as shown in Fig. 1(a). A vertical electric field of +2.6 kV/cm can be generated by applying a negative bias to the top electrode of the sample. As shown in Fig. 4(a), as the positive electric field gradually increases, the intersecting hump-like features are obviously suppressed and the ρ_{xy}^{AHE} are enhanced. On the contrary, the intersecting hump-like features can be clearly observed in the downward polarization under a negative electric field, which is consistent with the pristine state. It is worth noting that the magnitude of ρ_{xy}^{AHE} is larger than that of the pristine state whether this electric field is −2 kV/cm or −2.6 kV/cm. This can be understood from the fact the pristine state is not in fully downward polarization. Using a piezoelectric force microscope, the spontaneous polarization of PZT can be well-oriented and switched. The out-of-plane phase images are acquired after applying a written bias of ±8 V to a PFM tip over an area of 3 μm×3 μm. In Fig. 4(g), we show that the pristine ferroelectric polarization is downward. Figure 4(h) shows the phase images of the PZT film after being polarized with an electric field of +2.6 kV/cm generated by a negative bias. We observed that the phase images of the central region with −8 V applied are almost completely the same as those of the unbiased region, and the phase flip contrast of the PZT film is close to 180°, indicating that the PZT film can be completely polarized under an electric field of +2.6 kV/cm, and the polarization direction is vertically upward. Then, we apply the negative bias to the bottom electrode. As shown in Fig. 4(i), the phase images of the PZT film after being polarized with an electric field of −2.6 kV/cm. We observed that the phase images of the central region with −8 V applied are almost completely the same as those of the unbiased region, indicating that the polarization direction of the PZT film is reversed downward under an electric field of −2.6 kV/cm.

As shown in Fig. 4(a), the intersecting hump-like features are obviously suppressed or strengthened by applying a positive electric field or a negative electric field, respectively. More importantly, at a high magnetic field of −9 T, the sign of ρ_{xy}^{AHE} is reversed from negative to positive at the positive electric field. Furthermore, when the electric field is switched back to the negative electric field, the sign of ρ_{xy}^{AHE} is reversed from

positive to negative. As shown in Fig. 4(b), the MR curves of SRO/PZT/LSMO heterostructures also have corresponding features in the magnetic field region where the intersecting hump-like features appear in the ρ_{xy}^{AHE} curves. At the same time, the intersecting features can be clearly seen to disappear or appear by applying positive electric field or negative electric field, respectively. Figure 4(c) shows the electric-field dependence of $\sigma_{xy}^{\mathrm{AHE}}$ ($\sim -\rho_{xy}^{\mathrm{AHE}}/\rho_{xx}^{2}$) for the SRO/PZT/LSMO heterostructures at 40 K. Similarly, the sign of $\sigma_{xy}^{\mathrm{AHE}}$ (taken at -9 T) remains positive at the negative electric fields and turns negative at the positive electric fields. Compared with the value of $\sigma_{xy}^{\mathrm{AHE}}$ at a zero electric field, it reduces by about 19.4% at the electric field of -2.6 kV/cm but 483.3% at the electric field of $+2.6$ kV/cm, respectively.

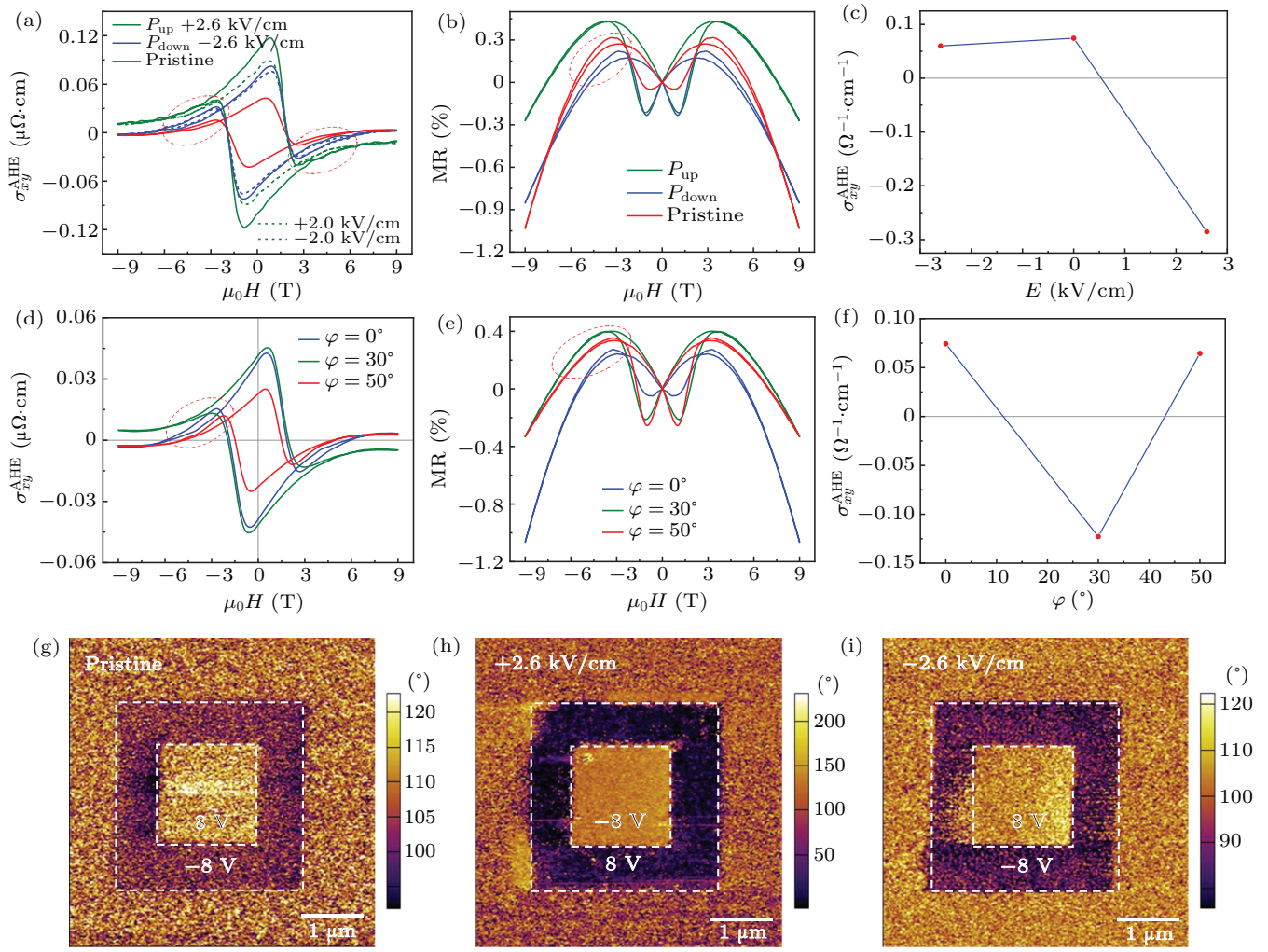


Fig. 4. Magnetic field-dependence of (a) ρ_{xy}^{AHE} and (b) MR of SRO/PZT/LSMO heterostructures under various electrical fields at 40 K. (c) Electric field dependence of the anomalous Hall conductivity $\sigma_{xy}^{\mathrm{AHE}}$ for SRO/PZT/LSMO heterostructures at 40 K with $\mu_0 H = -9$ T. Angular φ dependence of (d) ρ_{xy}^{AHE} and (e) MR of SRO/PZT/LSMO heterostructures under various electrical fields at 40 K. (f) Angular φ dependence of the anomalous Hall conductivity $\sigma_{xy}^{\mathrm{AHE}}$ for SRO/PZT/LSMO heterostructures at 40 K with $\mu_0 H = -9$ T. PFM out-of-plane phase images (g) pristine, at (h) +2.6 kV/cm and (i) −2.6 kV/cm.

In view of the fact that strain controls magnetic easy axis,[29] it is speculated that the sign reversal and the intersecting hump-like features of the ρ_{xy}^{AHE} are related to the magnetization rotation. To further clarify the contribution of magnetization rotation to the ρ_{xy}^{AHE}, the AHE is measured under inclined magnetic fields at an angle of φ with respect to the normal of films. In Fig. 4(d), the intersecting hump-like features are obviously suppressed at a small tilting angle ($\varphi = 30°$), while a large tilting angle ($\varphi = 50°$) leads the intersecting hump-like features to reappear. Similarly, in Fig. 4(e), the intersecting features of the MR curves are obviously suppressed at a small tilting angle ($\varphi = 30°$), while a large tilting angle ($\varphi = 50°$) leads the intersecting features to reappear. It should be noted that the change characteristics of angle-dependent AHE and MR are consistent with the those of AHE and MR modulated by external electric fields. Based on the angle-dependent AHE measurement, the intersecting hump-like features are indeed related to the magnetization rotation. The $\sigma_{xy}^{\mathrm{AHE}}$ is very sensitive to the angle (α) between the magnetization and the out-of-plane sample normal, exhibiting non-monotonical dependence, which should be attributed to the fact that Fermi level and electronic band structure are modified

with the Zeeman energy.[29] With the increase of the magnetic field, SRO forms a spin canting state and the magnetization tends to align with the external magnetic field direction, albeit with some deviations.[43]

The sign of the $\sigma_{xy}^{\mathrm{AHE}}$ is reversed from positive to negative as angle φ increases from 0° to 30° in a high magnetic field of −9 T, and subsequently the sign is reversed back to positive when the angle continues to increase to 50° as shown in Fig. 4(f). Again, the modulation of the electric field is related to the rotation of the magnetization. Specifically, the intrinsic contribution of AHE is determined by the integrating Berry curvature over all the occupied electronic bands in the entire Brillouin zone.[47] The intrinsic $\sigma_{xy}^{\mathrm{AHE}}$ of SRO is related to its Berry curvature of the underlying electronic structure:

$$\sigma_{xy}^{\mathrm{AHE}} = -\frac{e^2}{\hbar}\int_{B_z}\frac{\mathrm{d}k}{(2\pi)^3}\Omega^z(k), \tag{2}$$

where $\Omega^z(k)$ is the z-component of the Berry curvature.[1] The Berry curvature can also be modulated by rotating magnetization.[29] Therefore, the sign change of $\sigma_{xy}^{\mathrm{AHE}}$ in SRO/PZT/LSMO heterostructure may be closely related to the electronic band structure with the Zeeman energy. The rotation of magnetization in real space leads to Berry curvature evolution. These results demonstrate that the electric-field-induced sign reversal of the $\sigma_{xy}^{\mathrm{AHE}}$ (taken at −9 T) and the intersecting hump-like features are indeed related to the magnetization rotation. Therefore, the electric field can effectively modulate the Berry curvature through the magnetization rotation, which provides a material basis for the application of spintronic devices.

4. Conclusions

In summary, SRO films with in-plane tensile strain can be obtained by epitaxial growth of LSMO and PZT layers on STO substrates. The anisotropic magnetoresistance of the SRO/PZT/LSMO heterostructure exhibits a four-fold symmetric in a high magnetic field of 8 T. Furthermore, the anomalous Hall resistivity of the SRO/PZT/LSMO heterostructure exhibits a nonmonotonic behavior with the magnetic field. In a high magnetic field of −9 T, the sign of anomalous Hall conductivity is reversed owing to the change of electric field. The experimental results suggest that these interesting physical phenomena induced by electric field are attributed to the rotation of magnetization, which results the evolution of the Berry curvature. This work provides a controllable approach for modulating the magnetization and AHE in $SrRuO_3$ based heterostructures.

Acknowledgements

Project supported by the National Natural Science Foundation of China (Grant No. 11974099), the Intelligence Introduction Plan of Henan Province, China in 2021 (Grant No. CXJD2021008), the Plan for Leading Talent of Fundamental Research of the Central China in 2020, and the Key Scientific Research Project of Colleges and Universities in Henan Province, China (Grant No. 21A140005).

References

[1] Xiao D, Chang M C and Niu Q 2010 *Rev. Mod. Phys.* **82** 1959
[2] Bruno P, Dugaev V K and Taillefumier M 2004 *Phys. Rev. Lett.* **93** 096806
[3] Jiang W, Zhang X, Yu G, Zhang W, Wang X, Jungfleisch M B, Pearson J E, Cheng X M, Heinonen O, Wang K L, Zhou Y, Hoffmann A and te Velthuis S G 2017 *Nat. Phys.* **13** 162
[4] Shi Z L, Charles R, Cristian D B and Avadh S 2013 *Phys. Rev. Lett.* **110** 207202
[5] Itoh S, Endoh Y, Yokoo T, Ibuka S, Park J G, Kaneko Y, Takahashi K S, Tokura Y and Nagaosa N 2016 *Nat. Commun.* **7** 11788
[6] Zhong S, Orenstein J and Moore J E 2015 *Phys. Rev. Lett.* **115** 117403
[7] Everschor-Sitte K and Sitte M 2014 *J. Appl. Phys.* **115** 172602
[8] Wang G Q, Sun Z H, Si X Y and Jia S 2020 *Chin. Phys. B* **29** 077503
[9] Zhang D, Wang Y, Lu N, Sui X, Xu Y, Yu P and Xue Q K 2019 *Phys. Rev. B* **100** 060403
[10] Wang Q, Yin Q W and Lei H C 2020 *Chin. Phys B* **29** 017101
[11] Fang Z, Nagaosa N, Takahashi, K S, Asamitsu A, Mathieu R, Ogasawara T, Yamada H, Kawasaki M, Tokura Y and Terakura K 2003 *Science* **302** 92
[12] Yao Y G, Kleinman L, MacDonald A H, Sinova J, Jungwirth T, Wang D S, Wang E G and Niu Q 2004 *Phys. Rev. Lett.* **92** 037204
[13] Haldane F D M 2004 *Phys. Rev. Lett.* **93** 206602
[14] Lu W, Song W, Yang P, Ding J, Chow G M and Chen J 2015 *Sci. Rep.* **5** 10245
[15] Lee B W and Jung C U 2010 *Appl. Phys. Lett.* **96** 102507
[16] Ziese M, Vrejoiu I and Hesse D 2010 *Phys. Rev. B* **81** 184418
[17] Zayak A T, Huang X, Neaton J B and Rabe K M 2008 *Phys. Rev. B* **77** 214410
[18] Xu R, Huang J, Barnard E S, Hong S S, Singh P, Wong E K, Jansen T, Harbola V, Xiao J, Wang B Y, Crossley S, Lu D, Liu S and Hwang H Y 2020 *Nat. Commun.* **11** 3141
[19] Wu L, Wen F, Fu Y, Wilson J H, Liu X, Zhang Y, Vasiukov D M, Kareev M S, Pixley J H and Chakhalian J 2020 *Phys. Rev. B* **102** 220406
[20] Jia Q X, Foltyn S R, Arendt P N, Groves J R, Holesinger T G, Hawley M E and Lu P 2002 *Appl. Phys. Lett.* **81** 4571
[21] Ohuchi Y, Matsuno J, Ogawa N, Kozuka Y, Uchida M, Tokura Y and Kawasaki M 2018 *Nat. Commun.* **9** 213
[22] Qin Q, Liu L, Lin W, Shu X, Xie Q, Lim Z, Li C, He S, Chow G M and Chen J 2019 *Adv. Mater.* **31** 1807008
[23] Lu J, Si L, Zhang Q, Tian C, Liu X, Song C, Dong S, Wang J, Cheng S, Qu L, Zhang K, Shi Y, Huang H, Zhu T, Mi W, Zhong Z, Gu L, Held K, Wang L and Zhang J 2021 *Adv. Mater.* **33** 2102525
[24] Wang L, Feng Q, Kim Y, Kim R, Lee K H, Pollard S D, Shin Y J, Zhou H, Peng W, Lee D, Meng W, Yang H, Han J H, Kim M, Lu Q and Noh T W 2018 *Nat. Mater.* **17** 1087
[25] Yao X K, Wang C, Guo E J, Wang X Y, Li X M, Liao L, Zhou Y, Lin S, Jin Q, Ge C, He M, Bai X D, Gao P, Yang G Z and Jin K J 2022 *ACS Appl. Mater. Interfaces* **14** 6194
[26] Kan D, Kobayashi K and Shimakawa Y 2020 *Phys. Rev. B* **101** 144405
[27] Ren Z Y, Shao F, Liu P F, Wang M X, Chen J K, Meng K K, Xu X G, Miao J and Jiang Y 2020 *Phys. Rev. Appl.* **13** 024044
[28] Mizuno H, Yamada K T, Kan D, Moriyama T, Shimakawa Y and Ono T 2017 *Phys. Rev. B* **96** 214422
[29] Tian D, Liu Z, Shen S, Li Z, Zhou Y, Liu H, Chen H and Yu P 2021 *Proc. Natl. Acad. Sci. USA* **118** e2101946118
[30] Gao Z M, Huang X S, Li P, Wang L F, Wei L, Zhang W F and Guo H Z 2018 *Adv. Mater. Interfaces* **5** 1701565
[31] Zayak A T, Huang X, Neaton J B and Rabe K M 2006 *Phys. Rev. B* **74** 094104
[32] Felner I, Nomura K and Nowik I 2006 *Phys. Rev. B* **73** 064401

[33] Gausepohl S C, Lee M, Char K, Rao R A and Eom C B 1995 *Phys. Rev. B* **52** 3459
[34] Wakabayashi Y K, Kaneta-Takada S, Krockenberger Y, Taniyasu Y and Yamamoto H 2021 *ACS Appl. Electron. Mater.* **3** 2712
[35] Kan D, Aso R, Kurata H and Shimakawa Y 2013 *J. Appl. Phys.* **113** 173912
[36] Herklotz A, Kataja M, Nenkov K, Biegalski M D, Christen H M, Deneke C, Schultz L and Doerr K 2013 *Phys. Rev. B* **88** 144412
[37] Xiao X, Li J X, Ding Z and Wu Y Z 2015 *J. Appl. Phys.* **118** 203905
[38] Rout P K, Agireen I, Maniv E, Goldstein M and Dagan Y 2017 *Phys. Rev. B* **95** 241107
[39] Gong J L, Zheng D X, Li D, Jin C and Bai H L 2018 *J. Alloys Compd.* **735** 1152
[40] Camley R E and Barnas J 1989 *Phys. Rev. Lett.* **63** 664
[41] Rushforth A W, De Ranieri E, Zemen J, Wunderlich J, Edmonds K W, King C S, Ahmad E, Campion R P, Foxon C T, Gallagher B L, Vyborny K, Kucera J and Jungwirth T 2008 *Phys. Rev. B* **78** 085314
[42] Li P, Jiang E Y and Bai H L 2010 *Appl. Phys. Lett.* **96** 092502
[43] Chen X G, Yang J B, Yang Y B, Wang C S, Liu S Q, Zhang Y, Han J Z and Yang Y C 2014 *J. Appl. Phys.* **115** 043904
[44] Koster G, Klein L, Siemons W, Rijnders G, Dodge J S, Eom C B, Blank D H A and Beasley M R 2012 *Rev. Mod. Phys.* **84** 253
[45] Ding J J, Wu S B, Yang X F and Zhu T 2015 *Chin. Phys. B* **24** 027201
[46] Matsuno J, Ogawa N, Yasuda K, Kagawa F, Koshibae W, Nagaosa N, Tokura Y and Kawasaki M 2016 *Sci. Adv.* **2** e1600304
[47] Nagaosa N, Sinova J, Onoda S and MacDonald A H 2010 *Rev. Mod. Phys.* **82** 1539